Chemical and Optical Properties of CdSe and CdSe/ZnS Nanocrystals Investigated Using High-Performance Liquid Chromatography

Jess P. Wilcoxon* and P. P. Provencio

Nanostructures and Advanced Materials Chemistry, Department 1122, Sandia National Laboratories, Albuquerque, NM 87185-1421

Received: January 5, 2005; In Final Form: May 12, 2005

We apply a variety of characterization tools, including dynamic light scattering (DLS), transmission electron microscopy (TEM), high-resolution size-exclusion chromatography (HRSEC), and X-ray fluorescence (XRF), to study CdSe and CdSe/ZnS semiconductor nanocrystals of various sizes. We compare the size monodispersity, composition, and optical properties such as absorbance, photoluminescence (PL), and photoluminescence excitation of samples synthesized by high-temperature organometallic decomposition methods to CdSe clusters synthesized in our laboratory using a room-temperature metathesis from ionic precursors in coordinating solvents. DLS revealed considerable aggregation in all the conventionally synthesized samples, while TEM showed significant size and shape polydispersity in the core/shell CdSe/ZnS nanoparticles. We demonstrate how HRSEC can be used to explore size and shape polydispersity in semiconductor nanocrystals by measurement of the spectral homogeneity of the PL and PLE of spectra obtained within cluster elution peaks observed by HRSEC. Using HRSEC, we show that size fractionation by solvent/nonsolvent precipitation is only partially effective in size selection and that discrete size populations are present in each fraction. HRSEC shows that our synthesis yields a single-size, blue-emitting, homogeneous population whose absorbance and PL correspond to those of the smallest-size fraction made by conventional synthesis. This suggests that especially stable discrete sizes are favored in both synthetic methods.

Introduction

Type II−VI semiconductor nanocrystals are the most studied of all nanosize materials—sometimes called quantum dots (QDs). In fact, an early review article by one of the pioneers in this field indicates the remarkable amount of knowledge concerning their physicochemical properties even prior to 1990.[1] In the next decade, as improved synthetic methods—especially those using either inverse micelles[2a,b] or high-temperature decomposition in the presence of surface-active ligands[3]—became available, improved sample quality led to a plethora of new studies and an improved understanding of the relationship of size to optical properties.[4]

The refinement of synthetic protocols for making CdSe QDs using metallo-organic precursors has recently made solutions of such QDs commercially available. This will presumably allow their use by researchers who do not wish to train themselves as organometallic chemists. Additionally, since synthesis of CdSe QDs typically requires the use of extremely toxic, expensive, and pyrophoric reagents such as dimethyl cadmium, this commercial availability will improve safety. Some improvement in safety has recently been introduced into these methods by using cadmium acetate or CdO as the cadmium source, but it is not clear that the sample quality or product yield is as good with this substitution.[5]

Interestingly, though CdSe QDs are among the most studied of all nanocrystals, certain properties such as composition (that is, the Cd/Se ratio) as a function of size have not been reported. How the Cd/Se ratio, as well as how various ligands or solvents affect the optical properties such as PL energy and fluorescent yield, thus remain largely unexplored. The issue of composition is particularly important in the case of core/shell-type nanoparticles where one cannot be certain that all of the shell material is heterogeneously and uniformly deposited on the core nanocrystals.[6a,b] An assumption of full deposition onto the seed particles, as is commonly done, could result in a calculated shell thickness not corresponding to reality.

Part of the difficulty with investigations of the size-dependent optical properties of chemically synthesized nanocrystals is that one must obtain chemically pure samples of nanocrystals where size, shape, or compositional differences between nanocrystals in an ensemble have been eliminated by some type of selection or purification technique. Solvent/nonsolvent precipitation using, for example, hexane/pyridine, is commonly employed, but as we demonstrate in this paper using size-exclusion liquid chromatographic separation (SEC), this approach is only partially effective. Also, one cannot have residual precursor or excess ligands present if valid conclusions regarding the intrinsic properties of the QDs are to be obtained, so a way of separating these chemicals from the clusters is useful. In this paper we use SEC for this selection and characterization purpose for the first time. We combine these studies with solution measurements of elemental composition by X-ray fluorescence.

We examine the size-dependent optical properties of a series of CdSe nanocrystals synthesized by high-temperature organometallic precursors purchased from Evident Corporation. Each sample shows a significantly different emission color and onset of its optical absorbance, along with well-defined absorbance maxima arising due to discrete energy transitions, just as in research grade samples. However, unlike our n-CdSe sample prepared by room-temperature metathesis from ionic precursors

* Corresponding author. Tel: (505) 844-3939. Fax: (505) 844-4045. E-mail: jpwilco@sandia.gov.

10.1021/jp050062h CCC: $30.25
Published on Web 06/17/2005

in a coordinating solvent, these ensemble average absorbance properties can be due to two or more discrete cluster sizes, as we show with chromatographic analysis of the spectral properties of subpopulations in each fraction.

We also examine two samples of CdSe/ZnS core/shell particles with structured absorption features and blue and yellow PL, respectively. These samples show considerably larger (2−5-fold) fluorescence quantum yield compared to the CdSe core particles, but they have surprisingly large Zn/Cd ratios, typically 20:1! DLS, TEM, and SAD show these samples to be dominated by aggregates of ZnS with a cubic phase encasing the minority CdSe clusters responsible for the visible PL. All samples, except the research grade sample studied, have excess Cd, and the samples having the shortest wavelength absorption onset have the largest Cd excess and the highest fluorescence quantum yield, Φ_F. We find that Φ_F of our blue-emitting CdSe sample increases with sample age at room temperature as do the sharpness of its structured absorbance features and absorbance onset.

Experimental Section

Synthesis. The methods used for CdSe synthesized by Evident technologies are described in the patent literature and closely follow literature methods using thermal decomposition of Cd and Se organometallic precursors in a high-boiling-point solvent such as trioctylphosphine oxide, TOPO, containing trioctyl phosphine (TOP) surfactant. TOP was detected by SEC (see below), confirming that a high-temperature organometallic route was used,[3] followed by solvent/nonsolvent fractionation of the polydisperse product. The detection of pyridine in all the fractions confirms that pyridine was used as the nonsolvent in this process and is difficult to effectively remove following cluster precipitation and redissolution of the clusters in toluene. It is likely that a precursor such as dimethyl cadmium or cadmium acetate is co-injected with a Se source such as TOPSe into a TOP/TOPO solvent at high temperature, as described in the literature and several patents.[5,7] The success of the size-selective fractionation is moot as indicated by the SEC analysis of each of the fractions possessing a distinct PL color.

The deposition of ZnS onto the CdSe core particles also likely follows literature procedures,[6a] since a large amount of pyridine was also detected. Pyridine is typically used under reflux to remove the protective TOP passivant prior to deposition of the ZnS from organometallic sources. The presence of large amounts of separate ZnS nanoparticles was evident in the commercial samples, on the basis of HPLC, XRF, and selected area electron diffraction.

The CdSe synthesized in our laboratory was made via a room-temperature metathesis method in which equal volumes of two solutions were rapidly mixed in an Ar-filled glovebox. The first solution was $Cd(NO_3)_2$ (0.01 M) in tetrahydrofuran (THF), which contained a Cd(II) chelator, 0.01 M TOPSe in TOP, while the second solution was Li_2Se (0.01 M) also in THF.[7] Slow, room-temperature growth of CdSe over a period of ∼1 week was observed which ultimately resulted in intense blue PL and multiple sharp absorption and PLE features from the light yellow solution. Pyridine at ∼10−20 vol % was also used to grow CdSe colloids from the same ionic precursors but using a combination of 10 vol % pyridine (coordinating) in 90 vol % methanol (noncoordinating) for each solution. This approach is similar to that described by Ridley and co-workers.[8] Following precipitation of the yellow CdSe nanocrystals from the methanol solution, we dispersed the CdSe precipitate in neat pyridine with magnetic stirring or sonication to etch and improve the optical properties with time, as demonstrated in our previous work.[8] In both our metathesis approaches, slow growth of the nanocrystals is essential to achieving good final optical properties.

Transmission Electron Microscopy. Bright-field TEM was done on a JEOL model EX microscope operating at 120 kV with a point-to-point resolution of approximately 9 Å. Magnifications of 50k× or 100k× were used to obtain diffraction contrast images. Selected area diffraction (SAD) on regions of the grid was obtained at 120 kV and a working distance of 20 cm between the sample and detector planes. A JEOL model 2010 was used to obtain high-resolution lattice fringe images at magnifications of 600k× or 800k×. A ∼2-μL drop of a ∼0.01 M (atomic molarity) cluster solution in toluene is applied to a holey carbon grid resting on absorbent filter paper which rapidly wicks away the solvent. This allows the clusters to be well-dispersed on the grid.

X-ray Fluorescence. Cd, Zn, Se, S, and P concentrations were determined using a QuantX X-ray fluorescence (XRF) instrument against known standards in the same organic matrix, toluene. The concentration of low-*Z* elements such as S and P are the most difficult to obtain with high accuracy. However, such large amounts of these elements were present in the commercial samples that concentration determinations proved facile.

Size-Exclusion Chromatography. An Agilent Corporation 1100 series high-pressure liquid chromatograph equipped with Degasser (model G1322A), Quaternary fluid pump (model G1311A), automated injector (model G1313A), and three detectors—a photodiode array absorbance (PDA) spectrometer (model G1315A), scanning fluorimeter (FL) (model G1321A), and differential refractive index detector (RI) (model G1382A)—were used to detect the elution (single-channel), and complete absorbance, PL, and PLE (real-time scanning mode) spectra of the nanoclusters. The FL detector has adjustable PMT gain and user-selectable excitation wavelength(s). Laser dyes such as coumarine 500 (Exciton Corp.) were used to verify the wavelength accuracy of the on-line spectrometers as well as to estimate the fluorescence yield as outlined in detail below. The FL detector uses an S20 type PMT for detection of the fluorescence, and this signal is normalized by the output from a reference diode located behind the flow cell to correct for changes in the excitation intensity with wavelength or lamp age. The dark signal from both the PMT and the reference photodiode are subtracted prior to this normalization. The resulting output signal, shown in all the PL spectra in this paper, is expressed in luminescence units, LU. The output of the FL detector saturates at around 300 LU corresponding to a count rate of approximately 3×10^6 c/s. The bandwidth of the emission monochromator is fixed at 20 nm which limits the ability to resolve sharp emission peaks compared to our conventional double-grating instrument.

Nanocluster standards such as Au stabilized with alkanethiols[8] were used to compare elution line widths (size-dispersion) of the semiconductor clusters with known, nearly monodisperse samples. Nonabsorbing organic chemicals, such as trioctyl phosphine, were detected with the RI detector. A high-resolution, Polymer's laboratory model PL50 cross-linked polystyrene column filled with 5-μm microgel particles was used to separate the nanoparticles. The number 50 in the model PL50 designation indicates the approximate size of the gel pores, 50 Å. PL1000 columns were also used as employed in previous work on nanosize Au and Ag clusters.[11]

To compare both dye samples and nanocluster samples in a common solvent and optimize the symmetry of the cluster

elution peaks, a tetrahydrofuran, THF, mobile phase was used instead of the toluene phase we have used previously with hydrophobic metal clusters. The calibration of this system with size standards has been described previously in two papers, where it was demonstrated that, in the absence of specific chemical interactions between the clusters and the column, the time, t, required for elution is related to the hydrodynamic diameter, D_h, of the cluster by $\log D_h \sim t$.[10,11] In the present case we have evidence of such specific chemical interactions so, although smaller clusters elute at longer times as expected for a SEC mechanism, no attempt was made to assign absolute hydrodynamic sizes. Instead, such sizes were determined, where technically feasible, by dynamic light scattering (see description below).

The hydrodynamic diameter is the sum of the inorganic core size as measured by TEM and the effective thickness of the organic shell in the THF mobile phase. This thickness will depend on the solvent environment, being different in THF than in toluene, for example. The passivating layer for these commercial clusters appears to be TOP or TOPSe, which does not adhere to the cluster surface to the same extent as we have found for metal nanoclusters stabilized with suitable alkanethiols, so a significant fraction of clusters stick to the solid-phase SEC medium. Work is underway to optimize CdS, CdSe cluster/column interactions as we have demonstrated for other semiconductor and metal clusters.[12] Adding a thiol or TOP to the mobile phase improves the cluster elution; however, alkanethiols can quench the PL of CdSe clusters, so this strategy was avoided in the present case. Also, unlike alkanethiols, we do not presently have enough different chain lengths of alkyl phosphines (only TOP and tributyl phosphine, TBP, have been studied), so the thickness of the organic layer remains to be determined for these type II−VI semiconductor quantum dots.

Dynamic Light Scattering (DLS). The intensity autocorrelation function of the scattered light from dilute solutions of nanoclusters was determined using a Brookhaven Instruments model 9000 autocorrelator. A He−Ne laser operating at 632.8 nm and an intensity of ~13 mW was used as a scattering excitation source, since this wavelength is far enough to the red to not be absorbed by the semiconductor clusters. The nanocluster samples were studied in 10-mm path length quartz cuvettes (Spectrosil). The quasi-elastically scattered light was collected perpendicular to the incident beam by a Thorn-EMI S20 type photomultiplier tube. Our measurements were restricted to larger hydrodynamic diameter, $D_h > 3$ nm (that is, a 1-nm core with a 2-nm shell) CdSe clusters due to the very weak scattering observed from fully dispersed solutions of smaller clusters. DLS was also used to determine D_h for the optically transparent polystyrene (PS) column calibration standards used to calibrate the SEC columns.

Absorbance and Photoluminescence. A Cary model 2300 UV−visible−NIR, dual beam spectrophotometer was used to measure the cluster absorption. Depending on CdSe concentration, samples were studied in either 2-mm or 10-mm path length cells, with background subtraction of the solvent contribution, under ambient $T = 20$ °C conditions. A SPEX fluorolog II spectrophotometer with Xe arc lamp excitation and a double-grating excitation and double-grating detection system was used to obtain fluorescence emission and excitation spectra and fluorescence quantum yields, Φ_f. An S20-cooled PMT was used for photodetection, and the spectra were corrected for PMT response where appropriate and necessary. The samples were diluted enough, (OD ~ 0.1−0.2 cm^{-1}), to eliminate self-absorption effects, present in the concentrated commercial samples. This is not an issue for our samples which have no overlap between absorption and emission spectra.

Measurement of Fluorescent Quantum Yield. Our SPEX Fluorolog II spectrometer was used to collect the PL spectra with a typical excitation wavelength of 365 nm to obtain the number of emitted photons for each absorbed photon, Φ_f. Standard dye solutions of coumarin-500 (10^{-6} M in MeOH) with an emission peak at 493 nm and Rhodamine 6G (10^{-6} M in ethylene glycol) with an emission peak at 575 nm were used to obtain Φ_f, using literature values of $\Phi_f = 0.9$ and 0.95, respectively.[11a,b] The optical densities of the dye and cluster samples were adjusted to match at the excitation energy, eliminating corrections for light collection geometry. Dilute solutions of nanoclusters (OD ~ 0.1−0.2 cm^{-1} at 365 nm) held in 10-mm cuvettes were used. The emitted spectral energy distribution of the unknowns and reference standards were corrected for the response of our cooled S20 PMT detector. The total number of emitted photons was obtained for both unknown and reference standards from the area under the spectral energy distribution and, if necessary, normalized by the small differences (that is, OD differences on the order of 0.01 to 0.05) in optical density or number of photons absorbed at the excitation wavelength.

Results and Discussion

Figure 1 shows the ensemble average absorption spectra collected using our Cary 2300 spectrometer from a series of Evident (EV) CdSe clusters, freshly prepared in 10-fold diluted form in toluene. The cadmium concentration, [Cd], for each sample as received from the manufacturer is indicated in Table 1, which summarizes the chemical and optical properties of these clusters. The label for each sample is indicated in Table 1 and in this figure as EV1−EV5 (Evident samples 1−5), each sample having a lower energy absorption onset, first exciton transition, and PL energy as the cluster size increases. The chemical analysis in Table 1 originates from XRF measurements, while the optical properties were determined from the average spectra obtained from ensemble average measurements on our Cary 2300 or SPEX Fluorolog II spectrometers. The spectra in Figure 1 were obtained from samples diluted 10-fold and, combined with the [Cd] reported in Table 1, allow the molar extinction of each sample to be determined.

Multiple transition features are observed in the ensemble averaged absorption spectra shown in Figure 1a. One might conclude that the multiple absorption features reflect a narrow size dispersion of CdSe clusters with systematically larger sizes. Indeed, the peak wavelength of the first absorption feature shown in Table 1 increases from 520 nm (sample EV1, green-emitting) to 626 nm (EV5, red-emitting). The first absorption peak measured by us agrees with that specified by the manufacturer on their Website. However, the very strong overlap, as shown in Figure 1b, between absorption and emission means that the color of the solution is strongly weighted by the emission from the largest clusters in the ensemble and may not truly reflect the shapes or chemically distinct cluster surfaces present.

To examine the cluster dispersion, we performed HRSEC analysis of the CdSe cluster fractions to determine the homogeneity of the spectral properties of each sample. Spectra purity or homogeneity is an established approach to determine if an eluting peak contains more than one type of analyte.[14] A small pore size PL50 column was used in this analysis to ensure separation of all the small molecules, including unbound surfactants such as pyridine, TOP, and TOPO, from the clusters

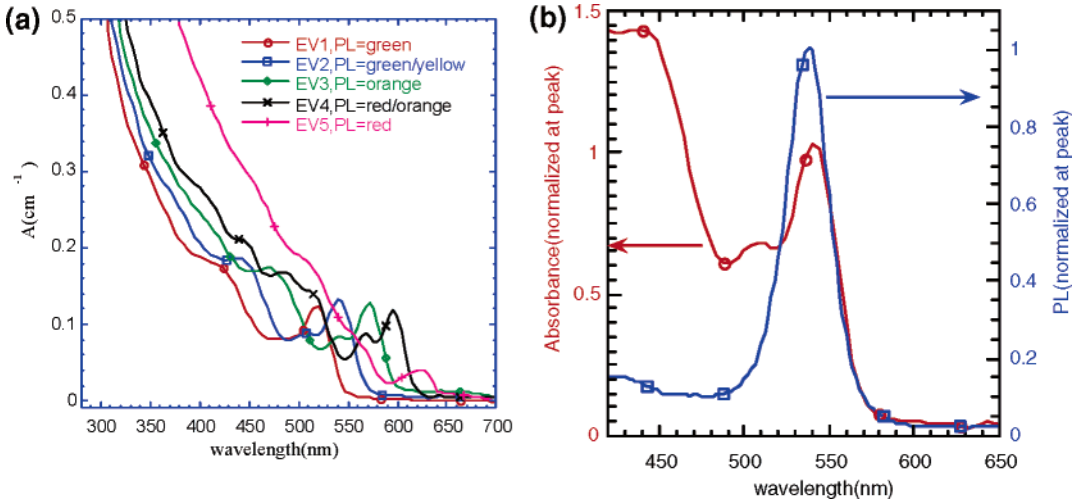

Figure 1. (a) Ensemble average absorbance spectra of CdSe cluster fractions EV1−5. (b) Coplot of ensemble average absorbance and emission of fraction EV2.

TABLE 1: Chemical and Optical Properties of the CdSe Samples

sample name	PL color	abs peak (nm)	PL peaks (nm)	[Cd] (M)	Cd/Se	Zn/Cd	[Cd+Zn]/[S]	Φ_f[a]
CdSe EV1	green	520	530	0.00251	1.82	NA	NA	0.059
CdSe EV2	green/yellow	540	517, 557	0.00262	1.52	NA	NA	0.047
CdSe EV3	orange	572	515, 586	0.00299	1.35	NA	NA	0.038
CdSe EV4	orange/red	596	514, 610	0.00340	1.51	NA	NA	0.025
CdSe EV5	red	626	519, 640	0.00571	1.26	NA	NA	0.029
CdSe/ZnS EV6	blue	460	482	0.00071	1.57	20.8	0.55	0.13
CdSe/ZnS EV7	yellow	530	475, 544	0.0011	2.1	17.2	0.50	0.23
CdSe 17	blue	406	464	0.005	1	NA	NA	0.32[b]

[a] Yield is obtained by comparison to either Coumarine dye with $\Phi_f = 0.90$ or Rhodamine 6G laser dye with reported yield of 0.95 [11a,b]. Optical density of the samples was adjusted to 0.1 cm^{-1} at the excitation wavelength of 365 nm. [b] After annealing under Ar at ambient temperature for 30 days.

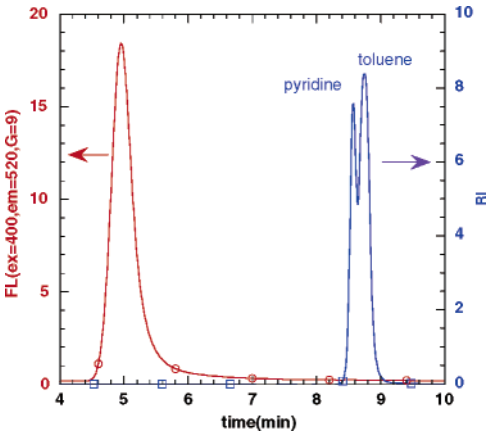

Figure 2. Fluorescence (FL) and refractive index (RI) chromatograms of CdSe sample EV1 showing clusters and solvent(s) separated. The column used was a PL50 type, and the mobile phase was THF flowing at 1 mL/min. The red trace is the output of the FL detector, and the blue trace is the RI detector signal.

and each other. The elution time of clusters and chemicals were monitored by absorbance, fluorescence (FL), and differential refractive index (RI).

Figure 2 shows a coplot of the FL and RI chromatograms from sample EV1, (green-emitting clusters). The fluorescence from the green-emitting clusters was monitored using the 520-nm channel of our multichannel scanning fluorimeter. Excitation was chosen at 400 nm and the emission was monitored at 520 nm. The refractive index signal shows the presence of two solvents, pyridine and toluene, in the sample. It is likely that the pyridine arises from a size-selective fractionation procedure involving a solvent/nonsolvent pair such as pyridine/hexane as described in the literature. However, the presence of pyridine negatively impacts the air stability of the samples. We discuss this issue more completely in our analysis of the CdSe/ZnS core/shell nanoparticles.

The broad width of the elution peak from this fraction was typical for these samples. To gain insight into the origin of this width (that is, size dispersion or chemical differences within the cluster population), we obtained full absorption and PL spectra throughout the elution peak(s) for each sample. These spectra were collected at intervals of ∼2−4 s which correspond to a size difference of ∼2−4 Å.[11] Figure 3 shows the absorption and PL spectra obtained at the peak of the elution for the EV1 sample with green emission. The PL spectra shown at the half-maximum height times are incompletely resolved (that is, mixed) cluster sub-populations. The peak apex time represents the numerical majority of the clusters, while the half width at half-height time indicates the spectral purity or homogeneity of the sample.

This EV1 sample likely corresponds to the last, smallest-size fraction to precipitate during size-selective purification and thus might be expected to be the most pure. We observe that there are two components in the PL spectrum, a strong green emission at 520−530 nm and significant near-UV PL between 400 and 450 nm. The peak observed near 400 nm does not shift with excitation wavelength, ruling out Raman scattering from a coeluting organic component. The absorption spectra are homogeneous throughout the peak, so only the peak apex spectrum is shown. This NUV PL would be missed if band-edge excitation at 500 nm were used in this experiment as is commonly done. NUV PL is present in all fractions and so may

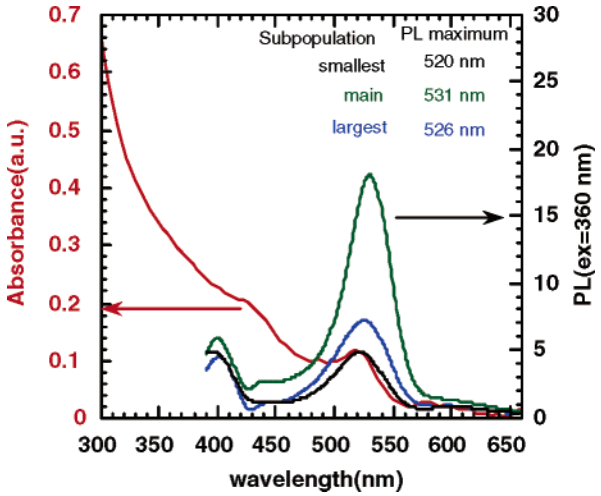

Figure 3. Coplot of absorbance (red curve) and PL at the elution peak time (green curve) and at the half width at half-height elution times (black, blue curves) from the fluorescence chromatogram of sample EV1 excited at 360 nm. The blue curve is the earliest-eluting component, while the black curve is the latest-eluting population.

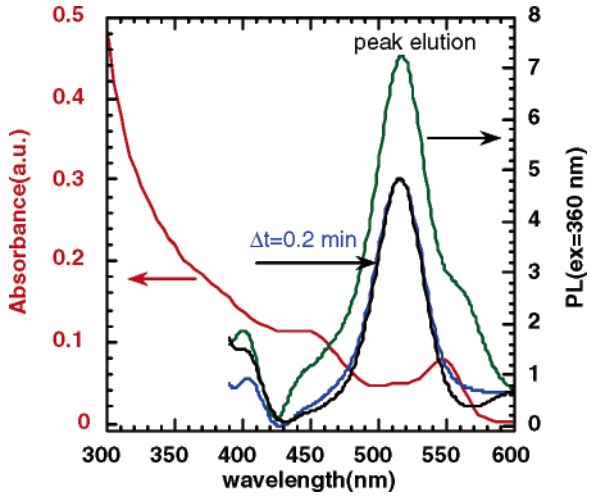

Figure 4. Absorbance (red curve) and PL at the elution peak time (green curve) and at the half width at half-height elution times (blue, black curves) from sample EV2 shows a main component and a shoulder in the visible PL when excited at 360 nm.

be either a coeluting chemical impurity or a sub-population of smaller, 1−2-nm CdSe clusters. The coelution of the sub-populations makes it impossible to collect separate, pure fractions for analysis by TEM. So we cannot rule out the possibility of a chemical contaminant adsorbed on the nanocluster surface being responsible for the PL in the 400−450-nm region. Figure 1b, obtained from sample EV2 on our conventional SPEX instrument using 360-nm excitation, confirms this NUV component.

The presence of a smaller sub-population of 1−2-nm CdSe clusters with NUV PL is most likely unless an unidentified organic passivating agent is present only on the cluster surface and is irreversibly bound. In all known cases of chemical passivation with surfactants or polymers, some of the passivant is free in solution and so would be separated from the clusters with bound surfactant by the column and elute as a separate peak. This peak should be detected in an absorbance chromatogram obtained using 360-nm light or a fluoresence chromatogram obtained using 360-nm excitation and detection of 400-nm emission. Figure 1 shows that chemical ligands such as pyridine are readily separated from the clusters and identified by RI detection. So, even though is it likely that a strong ligand such as pyridine coelutes with the CdS clusters, any unbound passivant or organic impurity will separate from the clusters during the chromatography analysis and should appear as a distinct PL peak in the 400−450-nm NUV region. This is not observed.

Figure 4 shows the absorption and PL spectra at the peak of the elution time for the EV2 sample with green/yellow emission. We observed two main features in the visible PL from the majority population, a strong green emission at ∼520 nm and a weaker shoulder at 557 nm, as indicated in Table 1. There is also PL from a coeluting sub-population emitting in the 400−450-nm near-UV region. The visible wavelength features originate from two distinct populations, and the PL from the samples eluting earlier and later in the peak lack the 557-nm shoulder. The first PL feature corresponds closely to the pure green peak observed in the smallest EV1 fraction (see Figure 3), while the 557-nm PL originates from a separate sub-population. Only this population emits light to the red of the absorption edge and thus dominates, while the shorter-wavelength PL is strongly absorbed. In fact, Figure 1b shows

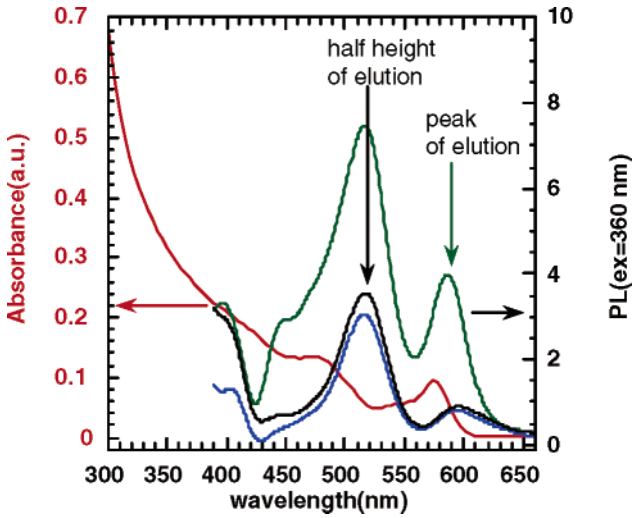

Figure 5. Absorbance and PL at the elution peak and at the half-width at half-height positions from sample EV3 shows two components in the PL when excited at 360 nm. The green curve is the PL spectra at the peak apex elution time, while the blue and black curves are obtained at the half-height elution times.

that the average emission peak from this sample occurs at 540 nm as a result of absorption of the shorter-wavelength emission.

Figure 5 shows absorption and PL spectral data obtained from sample EV3, an orange-emitting sample. The spectra were obtained at the peak elution and at the half-height positions. The elution peak is inhomogeneous, as indicated by the changing ratio of short, 515 nm, to the long, 586 nm, wavelength components. As in the case of EV2, one observes the presence of two distinct components in the PL spectrum, as noted in Table 1. There is also UV PL from a coeluting third component. The first visible PL peak, at 515 ×b1 5 nm, originates from the same discrete-sized sample population found in the PL spectrum of all the fractions, including the relatively pure fraction EV1; the second peak, at 586 nm, occurs to the red of the absorption and thus is not as strongly absorbed. It gives the sample its orange color despite the almost equal contributions from the two populations. We observe that the PL amplitude of each of the three components depends on elution time. For example, the spectral data from the earliest elution time (blue curve) has

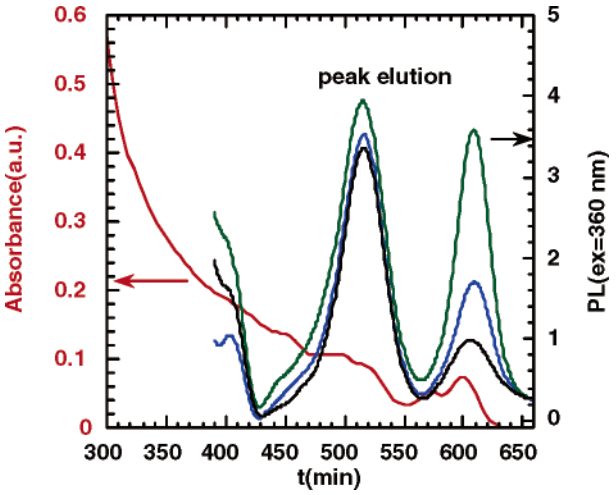

Figure 6. Absorbance and PL at the elution peak time and at the half width at half-height elution times from sample EV4 shows two components in the visible PL when excited at 360 nm. The green curve is the PL spectra at the peak, while the blue (short-time) and black (long-time) curves are obtained at the half-height elution times.

the least amount of 400−450 UV PL, consistent with this representing the largest size clusters in the coeluting population. The spectral data from the longest time elution of the profile (black curve) has the largest amount of near-UV PL and the least amount of orange PL, consistent with a smaller average cluster size.

The observation of at least two discrete populations with visible PL is also clear in the spectra of sample EV4. Figure 6 shows absorption and PL spectral data obtained from this sample. The spectra are shown both at the peak elution and at the half-height positions. The elution peak spectra are inhomogeneous, as indicated by the changing ratio of short, 514 nm, to the long, 610 nm, wavelength components with elution time. As in the case of samples EV2 and EV3, one observes the presence of two distinct components in the PL, as indicated in Table 1, as well as a component with near-UV PL. The smallest-size population, at 515 nm, originates from the same discrete-sized sample population found in the PL spectrum of all the fractions including the relatively pure fraction EV1, while the second, at 610 nm, occurs slightly to the red of the absorption and thus is not as strongly absorbed in an optically dense sample. It gives the undiluted sample its orange-red color despite the almost equal spectral contributions from the two populations. The earliest elution time spectral data (blue curve), which corresponds to the largest clusters for a SEC separation mechanism, contains the largest amount of orange-red PL, while the long-time spectral data (black curve) contains the largest amount of green PL.

The multiple features in the absorbance spectra shown in Figures 3−6 likely originate not from a continuous population dispersion but from at least two discrete ones—the original EV1 fraction with a first absorption peak at ∼520 nm and a second population of larger clusters with an absorption onset at longer wavelengths. Spectra were collected with 320-, 360-, and 400-nm excitation and only the relative intensities, not the peak positions, of the PL peaks depended on excitation wavelength. This change in relative PL peak intensity is expected due to the peaks observed in the PLE spectra from all samples. The presence of a subpopulation of even smaller clusters may be responsible for some of the structures observed in the absorbance in the 400−450-nm region. Thus, multiple distinct absorbance features in an ensemble average spectral measurement like Figure 1 do not necessarily imply a pure population of clusters if two or more discrete populations form during the synthesis. Only if a continuous range of sizes is formed will the transitions overlap sufficiently to wash out the distinct absorption peak transitions and create a featureless absorption spectrum.

What is the synthetic origin of this population inhomogeneity? We speculate that this may be due to incomplete fractionation during size-selective precipitation of the larger clusters from the smaller ones. In other words, both discrete populations are precipitating during the fractionation process, though the supernatant is certainly being enriched in the smaller population.

Our chromatography indicates that discrete, rather than continuous, size distributions may occur during the high-temperature growth process. Optical absorption and PL reported on research grade samples also show especially abundant cluster populations with absorption features closely matching these samples.[3, 6a,b] In CdSe samples prepared by following literature protocols[6a,b] involving decomposition of dimethyl cadmium and TOPSe in TOP/TOPO, we typically observe some NUV PL when excited at 360 nm, just as in the commercial samples. However, its intensity relative to the main PL peak is usually smaller than that observed in Figures 3−6. Also, only a single PL peak from one cluster population is observed in the visible near 590 nm. Unlike the EV3 sample shown in Figure 5, the PL is mainly from a single peak centered at 590 nm, consistent with a more homogeneous population. Normalized absorbance and PL spectra obtained at the peak of the elution curve from this research grade sample are shown in Supporting Information, Figure 1S. Figure 1S shows evidence of another population of green-emitting clusters with a shoulder near 520−530 nm. For this sample it is known from the synthesis conditions that the main passivant is TOP, which has no absorbance at 360 nm nor emission in the NUV. However, if it forms a complex with another metal such as Cd near the cluster surface, unexpected NUV PL might be observed.

What do we know about the chromatographic separation mechanism for CdSe clusters stabilized with organic ligands such as TOP or pyridine? For Au clusters passivated by alkanethiols, we have demonstrated that a pure SEC mechanism holds and that one can obtain the hydrodynamic diameter (Au core + organic shell) of the clusters.[10] In Figure 7 we show chromatograms obtained with the three types of on-line detectors in our system for samples such as d = 2.0-nm Au (PDA detector), linear alkanes such as hexadecane (C_{16}), dodecane (C_{12}), and octane (C_8) (RI detector), and our research grade d = 1.8-nm CdSe/pyridine (CdSe 17, Table 1) (FL detector). All chromatograms were obtained using a PL1000 column with THF as the mobile phase. One notes that, with the larger 1000-Å pore size as compared to the 50-Å column whose data were shown in Figures 3−6, greater penetration and longer elution times are observed for each sample, as expected for the SEC mechanism. Furthermore, the molecules with the smallest hydrodynamic diameter, the alkanes, elute at the longest times. These retention times are well separated from the larger cluster samples as well as from each other. Moreover, the CdSe clusters synthesized in-house have an elution width comparable to the best Au standard(s) and are similar in width to the linear alkanes. Such a narrow width implies negligible size, shape, or chemical polydispersity in this sample, in contrast to those of the commercial clusters. Even so, a tailing is observed in the elution profile of our CdSe/pyridine clusters, indicating that the mobile-phase THF does not passivate the cluster sufficiently to prevent some chemical interactions with the column material. This results in a longer elution time than expected for a pure SEC

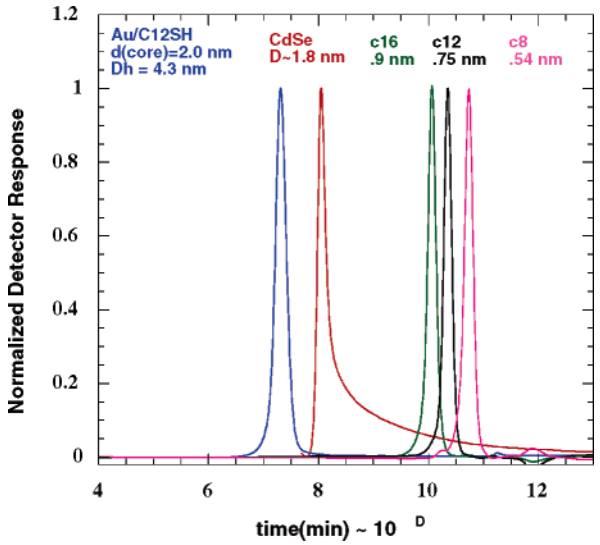

Figure 7. Normalized detector response vs elution or retention time for $d = 2.0$-nm Au/C12SH clusters (blue), $d = 1.8$-nm CdSe/pyridine clusters (red), and linear alkane standards such as hexadecane, C_{16}, (green), dodecane, C_{12}, (black), and octane, C_8, (pink). The column type is PL1000, and the mobile phase is THF flowing at 1 mL/min.

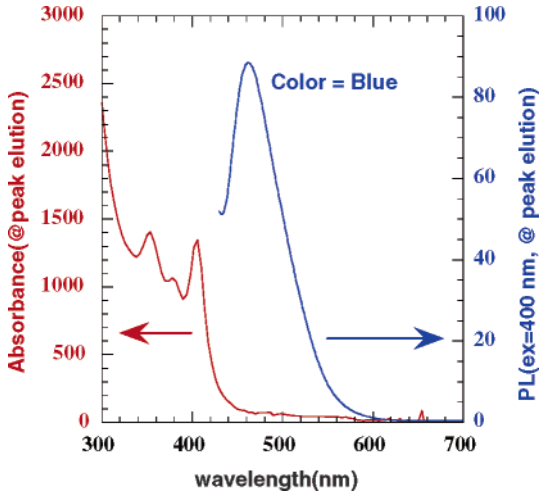

Figure 8. Coplot of the absorption and photoluminescence, PL spectra of the CdSe/pyridine, $d = 1.8$-nm cluster sample showing the sharp, homogeneous features at the peak of the elution chromatogram of Figure 7.

mechanism for the CdSe, 1.8-nm core cluster size. This size is consistent with HRTEM of this sample (see Supporting Information, Figure 2S).

A possible explanation for the longer elution time for the CdSe/pyridine compared to Au clusters of a similar core size may be a significantly larger organic "shell" around the CdSe clusters compared to the dodecanethiol used to passivate the Au standard. This does not seem likely, however. In the case of the Au/ dodecanethiol clusters shown, the hydrodynamic diameter is known to be 4.3 nm.[10] We do not know if the same organic thickness holds for the CdSe/pyridine clusters, so we cannot directly extract a core size for these clusters. Similar shell thickness uncertainties hold for our CdSe/TOP clusters synthesized in THF. We measure a DLS hydrodynamic diameter of 4.1 nm for CdSe/pyridine clusters, so we expect similar elution times for the two clusters. From the tailing of the elution peak, we conclude that chemically specific interactions are also contributing to the retention time of our CdSe/pyridine clusters.

The narrow elution peak of our CdSe 17 ($d = 1.8$ nm) sample synthesized by the metathesis process, compared to that of our commercial samples, suggests that the absorption and PL spectra should be homogeneous throughout the resolution-line width-limited elution profile of Figure 7. Indeed, this is the case. A single PL spectral shape is found throughout the elution, indicating a single population as shown in Figure 8. Moreover, the absorption spectrum shown in this figure exhibits sharp absorption peaks that are narrower than any of those of the commercial samples we investigated. Interestingly, the energies of these spectral features closely match those of the blue-emitting fraction first isolated by size-selected precipitation by Murray et al. (see Supporting Information, Figure 3S).[3] Although our blue-emitting sample has more spectral features than the 1.2-nm fraction isolated by Murray et al., the close agreement in the transition energies may indicate formation of an especially stable "magic"-size cluster, as has been suggested by other workers.[15] In this other work, a size of 1.7 nm was found to be especially stable and the absorption and PL were similar to those of our 1.8-nm clusters and Murray's $d = 1.2$-nm fraction.

The use of chromatographic separation of clusters combined with on-line analysis of the spectral homogeneity of both absorption and PL is a powerful method to evaluate the presence of size, shape, or chemical inhomogeneity in a sample of nanoclusters. It can also be used to obtain the relative fluorescence yield of clusters compared to organic dyes. Very small quantities of clusters are needed for a chromatographic/spectral analysis, typically 10 μL of a 0.005 M solution of CdSe. This means the spectra are obtained on very dilute concentrations of clusters, ~100 times less than the concentration of the parent solution at a flow rate of 1 mL/min. So self-absorption and concentration quenching effects are avoided, yielding the fluorescent yield for the ideal case of very low concentration. Thus, if one can perform chromatography on a reference sample such as a dye which is soluble in the same mobile phase as the nanoclusters, THF, one can compare the amount of PL (from the PL chromatogram at the peak emission or any other chosen wavelength) to the fraction of the excitation light absorbed (from the absorption chromatogram at the excitation wavelength) for both the CdSe clusters and the dye and obtain the fluorescence yield, Φ_f. In the case of the blue and blue-green-emitting clusters, a suitable THF-soluble reference dye is coumarine 500 (CM500) or 540 (CM540) (Exciton corporation). For orange- or red-emitting clusters, a suitable THF-soluble dye is DCM (Exciton corp.). Since $\Phi_f \sim 0.70$ for freshly prepared deoxygenated CM500 dye in ether (it is 0.9 in ethanol), we can obtain Φ_f for the sample shown in Figure 9. Here we have converted the absorbance chromatograms for CM500 dye and CdSe ($d = 1.8$ nm) to the fraction of light absorbed at 400 nm, the wavelength chosen for excitation of both the dye and the clusters.

The emission was monitored at the PL intensity peak of 470 nm for the clusters. A calculation of the ratio of the light emitted at the peak of the PL chromatogram (or alternatively the area under that chromatogram) to the fraction of light absorbed at the excitation wavelength of 400 nm yields a value of 4250 for the dye and 1275 for the clusters. The ratio of the areas is 0.3. Using a measured value of $\Phi_f = 0.7$ for the CM500 dye in THF, we obtain $\Phi_f = 0.21$ for the clusters. This value is slightly lower than the value of $\Phi_f = 0.32$ found by conventional measurements of dilute samples of CdSe 17 in pyridine (reported in Table 1) and may reflect a solvent dependence of the fluorescence yield for the clusters. Interestingly, a similar comparison of the fraction absorbed and PL chromatograms for CM500 and CM540 gives nearly identical values of the ratio

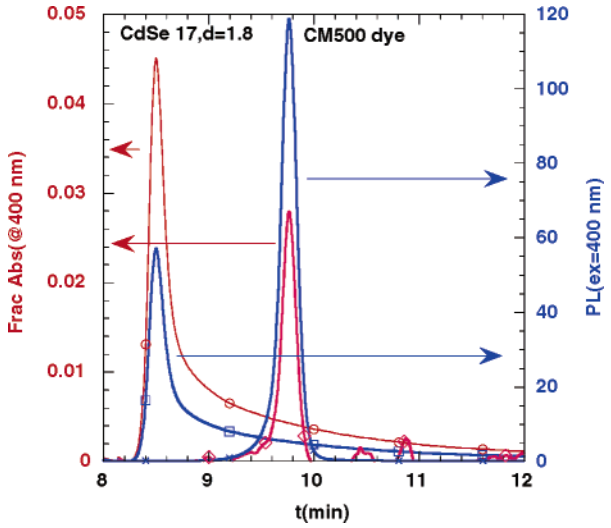

Figure 9. Coplot of the chromatograms for fraction of light absorbed at 400 nm (red curves) and PL emitted at the PL peak (blue curves) when excited at 400 nm for CM500 dye and CdSe 17, $d = 1.8$-nm clusters.

of light emitted at the peak to fraction absorbed, even though the peak emission of CM540 is red-shifted by 30 nm from the CM500 peak at 465 nm in THF. Thus, this method predicts that the fluorescent yield for CM540 is comparable to that of CM500 in THF. Φ_f for this dye in THF has not yet been reported.

Table 1 shows Φ_f measurements for each sample as measured using excitation at 365 nm. The commercial samples have values of Φ_f between 0.059 and 0.029 with a systematic decrease in Φ_f with red shift or increasing cluster size. Our results are consistent with the values reported by Murray et al. for CdSe prepared by high-temperature decomposition of $Cd(Me)_2$ and TOPSe.[4] These values ranged from 2 to 5%, depending on PL color.

The Φ_f of our sample prepared by metathesis is large for an unpassivated cluster. However, it does not reach this high value immediately following synthesis. In fact, no emission is observed a day or two after synthesis. Visible blue emission upon 365-nm Hg lamp excitation is observed under room lights only after ~7 days. With sample age, typically 30−45 days, a steady increase in Φ_f is observed and, provided no oxygen is present, retains this high value indefinitely.[8]

This increase in Φ_f with time is a general phenomenon observed in room-temperature synthesis of very small, $d <$ 2 nm, high-surface-area CdS and CdSe, and we have reported some of these effects in CdS previously.[8] It appears to be due to a surface restructuring mediated by the surfactant, in this case, pyridine. Much like the thiol-mediated etching phenomena demonstrated in nanosize Au clusters,[16] pyridine enables the facile movement and exchange of atoms between clusters, apparently optimizing the cluster size on the basis of thermodynamic stability. During these increases in PL intensity, the absorbance onset and physical size of the cluster as determined by TEM and SEC remain invariant. The width of the absorption transitions, however, usually decreases, and their relative amplitudes change.

Further insight into the factor(s) responsible for changes in Φ_f with time is obtained from DLS measurements of the apparent hydrodynamic diameter D_h of the clusters. In the case of our CdSe sample, large values of D_h were observed 1 day following dissolution of the methanol-induced precipitate from this sample in pure pyridine. Over time, D_h decreased, reaching a final value of 4−5 nm about 30−45 days following synthesis. This fully dispersed state correlates with the emergence of multiple sharp absorption feature(s), a distinct absorption onset, and larger Φ_f.

The agglomeration of individual clusters acts to quench the PL as expected, and this may partially account for the lower values found for Φ_f in the commercial samples. For each fraction of the commercial samples, one finds unrealistically large values of D_h compared to the expected nanometer size as gauged from the onset of the absorbance or TEM. Values for the commercial samples all exceeded $D_h = 20$ nm, consistent with agglomeration in solution, which was reflected by large amounts of electron scattering from films of these clusters prepared for TEM. DLS measurements obtained at the highest cluster concentrations showed the largest hydrodynamic sizes, consistent with increased cluster aggregation. This indicates the very large sizes measured reflect incomplete cluster dispersion, not simply the presence of an additional hydrodynamic shell of organic passivant on the cluster surface.

We tried to etch the commercial samples using pyridine, as was done for our sample, but we found that the etching was uncontrolled, blue-shifting the PL into the UV and nearly completely dissolving the clusters. Pyridine was also found to severely quench Φ_f from the core/shell samples (see below), as did the addition of alkanethiols. This indicates that the simple picture of a conformal shell of ZnS on CdSe is unlikely to be true. The pyridine clearly reaches the CdSe core surface responsible for the visible PL.

There is additional information in the elution-time-dependent measurement of Φ_f obtained using chromatographic separation combined with on-line absorbance and PL detection. If the cluster population and hence elution spectral profile is inhomogeneous, one learns about the relative contributions of individual sub-populations to Φ_f. Certain cluster subpopulations may have relatively more emitted light due to chemical, shape, or size differences. One can identify and even collect these subpopulations. We defer a detailed analysis of such inhomogeneous semiconductor subpopulations to a future publication. We simply note here that such inhomogeneity of Φ_f with elution time was quite common in these commercial samples. It is found to be homogeneous for expensive, chemically homogeneous laser dyes, as expected.

An interesting question is what is the structure of core/shell particles prepared by deposition of a material which has a significant lattice mismatch such as ZnS on CdSe? One might expect that even if very slow deposition to maximize heterogeneous deposition onto the core "seed" clusters is employed, a significant amount of homogeneous growth of the "shell" material as separate nanoclusters or islands on the core seeds might occur. The latter would give rise to nonspherical particles.

To investigate this issue, two CdSe/ZnS core/shell-type cluster samples, EV6, blue-emitting, and EV7, yellow-emitting, were investigated with the chemical and optical properties shown in Table 1. First, one notes a 2−5-fold increase in Φ_f compared to that of the corresponding core nanoparticles. This is consistent with other reports in the literature.[6a,b] Thus, at least some ZnS has deposited on the core seeds. XRF was used to determine how much Zn and S was present in the solution. To our surprise, a Zn/Cd ratio of nearly 20:1 was found for both EV6 and EV7. It is unreasonable that this much ZnS is present on the surfaces of the CdSe nanoparticles. However, when this result is considered in light of the large amounts of S detected, approximately twice the atomic amounts of Cd and Zn, it is

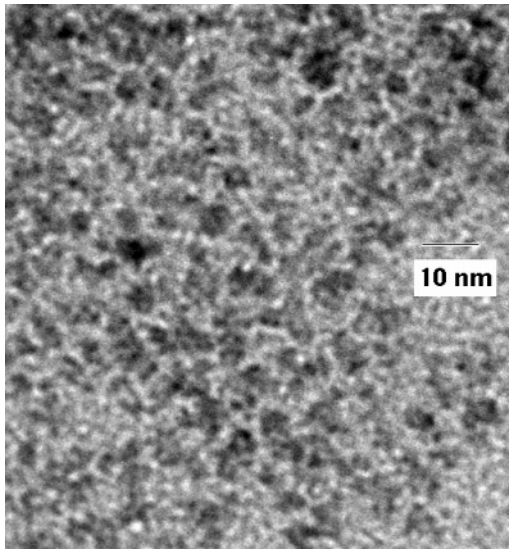

Figure 10. TEM of sample CdSe/ZnS EV6. The clusters of CdSe with sizes from 2 to 6 nm are embedded in a matrix which, from SAD, is likely ZnS.

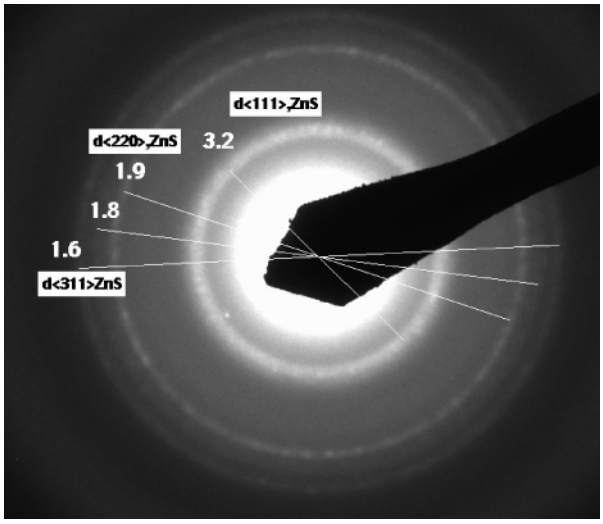

Figure 11. SAD from CdSe/ZnS EV6 shows that the majority of the diffraction from the above TEM region is from ZnS. The expected ZnS indexed reflections for the cubic phase are shown with the *d* spacings in Å.

likely that large amounts of ZnS clusters may be present in the solution. The Cd/Se ratio of 1.6 (EV6) or 2.1 (EV7) in these samples is similar or higher than that of the CdSe EV1−5 samples.

A TEM of sample EV6, Figure 10, shows that large amounts of another material are present around the darker CdSe clusters which range in size from 2 to 6 nm. Particles in the 1−2-nm range can also be observed in this TEM and in other regions not shown. CdSe with a size of 1−2 nm could account for the NUV PL observed in these samples. ZnS particles in this size regime would not absorb 360-nm excitation light and could not account for the NUV PL shown in Figure 13. We performed selected area electron diffraction (SAD) on this region of this grid. The aperture used for SAD probes diffraction from much larger areas, typically several square micrometers of the holey carbon grid, than shown in Figure 10. SAD in Figure 11 shows continuous diffraction rings matching the cubic bulk structure of ZnS. The index and *d* spacing for the rings is indicated in this figure. The *d* spacing is determined from the known sample-to-detector plane distance and wavelength of the electrons. The

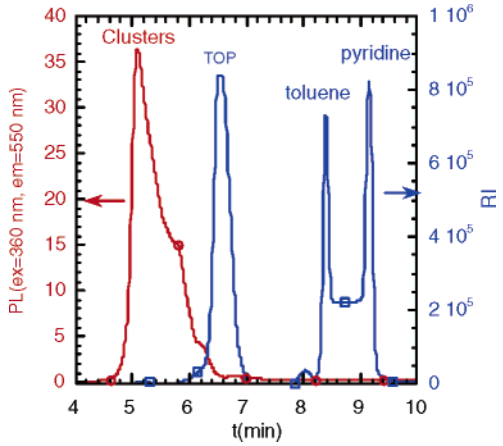

Figure 12. Absorbance at 360 nm and RI vs elution time for CdSe/ZnS EV7, green-yellow-emitting sample. The column used is a PL50 type, and the mobile phase is THF flowing at 1 mL/min. Fluorescence excitation is at 360 nm, and detection at 550 nm.

ZnS diffraction originates from the abundant lower-contrast material which surrounds the cores of the darker CdSe. A ∼2-nm core size would be consistent with the optical properties of blue-emitting CdSe. However, no CdSe diffraction was detected (that is, the $d\langle 111\rangle = 3.51$ Å for cubic CdSe is absent), which makes sense given the 20:1 Zn/Cd ratio found by XRF for this sample.

Consistent with the agglomerated appearance of the clusters in the TEM of Figure 10 is the large, hydrodynamic diameter of ∼30 nm measured by DLS. This large value indicates cluster aggregation even in solution. In addition, the decay of the intensity autocorrelation function from dilute solutions of both EV6 and EV7 was highly nonexponential, indicating more than one size of agglomerate.

The chromatography studies of both core/shell samples EV6 and EV7 gave similar results, and broad elution peaks were observed with a low efficiency of elution. The latter was likely due to the presence of large agglomerates which are effectively filtered out by small pore size of the column. The absorbance and PL showed spectral inhomogeneity, as did the core particles of EV1−EV5. We illustrate these results with EV7, whose PL and RI chromatograms on the PL50 column are coplotted in Figure 12.

There are several salient features in this chromatogram. One observes both pyridine and toluene (the cluster solvent) in the sample. Also, a new component whose retention time matches that of TOP was observed. This was not found in the chromatogram of EV1, Figure 1, but was present in the other fractions. Since XRF showed a [P] of nearly 0.1 M in this solution, such a large peak is not surprising. What is surprising is that this peak corresponds to TOP not TOPO, indicating that TOP is acting as the stabilizer for this sample. Furthermore, it must be present in overwhelming excess. Ligation of Cd sites on the Cd-rich surface is more reasonable than oxygen ligation since P is a better metal chelating atom than O. Recall that alkyl phosphines are used to dissolve metals such as Se or Te to form TOPSe(Te), the Se component in high-temperature organometallic synthesis of CdSe(Te). Our observations indicate it is likely that the assumption that TOPO stabilizes the surface of CdSe or CdSe/ZnS is incorrect. Also, the assumption that pyridine can be removed completely by washing with alcohols during size-selection procedures may not be warranted.

Additional evidence for the ligation of CdSe by TOP, not TOPO, comes from the following solubilization experiment.

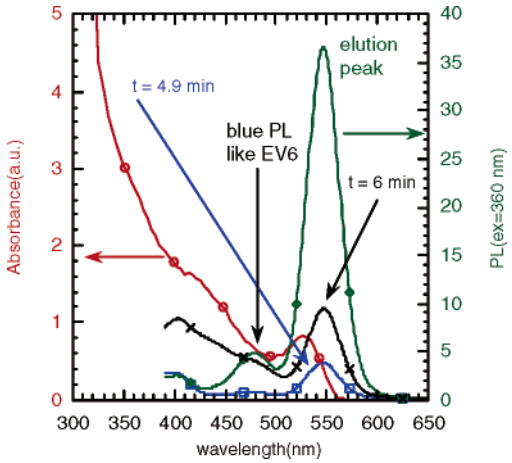

Figure 13. Coplot of absorption and PL excited at 360 nm vs wavelength for the elution peak (majority population), and spectra at $t = 4.9$ and $t = 6$ min (minority populations) for sample EV7.

After precipitation of our CdSe ($d = 1.8$ nm) sample from methanol, we attempted to dissolve the clusters in a noncoordinating solvent, toluene, containing either TOP or TOPO. We found that the latter (TOPO) failed to allow any CdSe nanoparticle solubility, while the former (TOP) formed a yellow transparent solution of CdSe/TOP after stirring. Using TOPSe/TOP was even more effective for solubilizing our CdSe ($d = 1.8$ nm) precipitated nanocrystals. This argues that the excess TOPSe commonly employed in high-temperature organometallic CdSe synthesis also ligates to sites on the Cd-rich surfaces.

The presence of pyridine in both EV6 and EV7 samples can be rationalized if, as has been reported in the literature,[6a,b] refluxing in neat pyridine of the CdSe/TOP seed nanoparticles is necessary prior to heterogeneous growth of ZnS. Pyridine is an excellent ligand for CdS and CdSe and so may still be present in abundance, as indicated in this chromatogram, if sufficient washing after precipitation is not done. An unfortunate aspect of having so much pyridine present in solution is that etching of the clusters upon air exposure will occur, meaning that even clusters with large amounts of ZnS will not be resistant to etching.

Unfortunately, the pure heterogeneous deposition of ZnS onto the CdSe seeds is only partially obtained, as indicated by the PL spectra within the cluster elution peak of sample EV7, Figure 12. One notes a substantial width to this peak in the region from 5.5 to 6.4 min. Figure 13 shows the absorbance and PL from the peak apex and the half width at half-height elution times of this peak.

In Figure 13, one observes that there are two components in the PL spectra and that the relative contributions of the yellow (~540 nm) and blue (~475 nm) components depend on elution time. The longest time, $t = 6$ min, corresponds to the smallest clusters in a pure SEC separation. Interestingly, it has the largest contribution of both blue and near-UV PL. The $t = 4.9$ min peak which corresponds to the largest clusters in a SEC separation shows only one PL peak at 540 nm. This cluster subpopulation may correspond to the most chemically pure portion of the sample, with ZnS deposited onto CdSe and no free ZnS. Even the majority population at the elution peak, however, shows the presence of both components. This indicates that the size-selection process to harvest only the yellow-emitting clusters of a fixed core size is difficult, as some of the smaller discrete population of blue-emitting clusters from fraction EV6 are still present.

DLS on the EV7 sample showed a very nonexponential decay and an apparent hydrodynamic diameter, even on a centrifuged sample, of over 200 nm, showing even more aggregation than the EV6 sample. This fraction, having a larger average size, is the precipitate in a precipitation purification step, and the large amounts of TOP present may indicate the difficulty of dispersing this precipitate in toluene. This is consistent with the large D_h measured.

The large amounts of ZnS found in this sample, as indicated by the 17:1 Zn/Cd ratio found by XRF (Table 1), suggest a fusion of clusters together, perhaps with deposited ZnS islands providing the "glue" to hold the aggregate structure together. Nevertheless, $\Phi_f = 0.23$ was similar to literature values for core/shell particles. The absorption spectra throughout the elution peak are quite homogeneous (see Supporting Information, Figure 4S) and structured, with a first absorption peak width comparable to most material reported in the literature. So, this association in solution does not quench the PL as much as might be expected.

As noted, despite the PL spectral inhomogeneity found in the broad elution peak of Figure 12, the absorption spectra are quite homogeneous, with a single absorption onset near 550 nm as shown in the Supporting Information, Figure 4S. This indicates that the absorption spectra are less sensitive to population inhomogeneity, especially when just two or three discrete populations are present, than the PL or PLE. In fact, in Figure 5S of the Supporting Information we show that the PLE is also quite inhomogeneous throughout the elution peak. This contrasts to our CdSe 17 ($d = 1.8$ nm) where absorption, PL, and PLE spectra are all homogeneous throughout the narrow elution peak

Conclusions

We have used several analytical methods to study the chemical and optical properties of both commercial and research grade CdSe nanocrystals. The commercial samples were made via high-temperature organometallic decomposition, followed by size-selective fractionation methods and showed aggregation in solution as monitored by DLS. Our blue-emitting CdSe ($d = 1.8$ nm) sample was made by a metathesis process at room-temperature from simple ionic salts in a 10 vol % pyridine in methanol solution with a 100% yield of a single size cluster with sharp HOMO−LUMO transitions. We discovered that the sharpness of these transitions, the state of dispersion of the clusters, and Φ_f all increased with aging in pyridine as a result of an etching/dissolution process.

It was discovered that each commercial fraction contained at least two discrete populations: one sub-population of the smallest clusters and the next subpopulation from the next larger cluster group. The PL energy from the larger cluster subpopulation lay slightly beyond the band edge absorption onset and gave the bulk sample its characteristic emission color. Evidence for significant amounts of smaller-size subpopulations of either clusters or chemicals with near-UV PL in the 400−450-nm range was found for all the commercial samples and particles in the 1−2-nm size range were observed in TEM images. We failed to observe a separate elution peak, due to a free, unidentified passivant, in chromatograms obtained using 360-nm excitation and 400-nm emission, further supporting our conclusion that the near-UV PL originates from a 1−2-nm CdSe cluster subpopulation.

Consistent with the two distinct peaks in the PL for three of the CdSe fractions investigated was a spectral inhomogeneity with elution time, suggesting coelution of two or more pop-

ulations. Later-eluting sub-populations, which represent the largest clusters in a pure SEC elution mechanism, showed a larger ratio of long-wavelength to short-wavelength PL. The absorption spectra, on the other hand, were quite homogeneous throughout the broad elution peak. So absorption measurements are less sensitive to population inhomogeneity if only discrete populations are present. It is possible that the PL inhomogeneity originates from either cluster-surface chemical inhomogeneity or cluster-shape differences rather than from a substantial average size difference.

Samples with a putative CdSe/ZnS core/shell structure were also investigated. It was discovered that, in addition to having Cd/Se > 1 for all the commercial samples, these samples had an extraordinarily high Zn/Cd ratio of ~20, inconsistent with the claimed shell thickness of a few monolayers. TEM and DLS showed large aggregates with a lower contrast material between the darker CdSe clusters. SAD was consistent with the high Zn and S values found by XRF, showing only cubic ZnS diffraction rings since CdSe was the minority component in these samples.

A surprising analytical result was the high amount of phosphorus, typically 0.1 M in the core/shell particles which were only $(1-5) \times 10^{-3}$ M in Cd. Supporting this observation were RI chromatograms which showed that TOP was the source of the phosphorus, not TOPO as is commonly assumed in the literature. We cannot rule out TOPO as a minority, coeluting component, however.

The strong air-sensitivity of Φ_f for the ZnS-coated particles could be explained by the observation of substantial amounts of pyridine in all of the commercial samples. Pyridine acts as an etchant in both our metathesis process and when used to remove the TOP prior to ZnS deposition during the commercial coating process.

Our 1.8 nm-CdSe clusters made via a room-temperature metathesis approach had a very narrow elution peak and were spectrally homogeneous in absorption, PL, and PLE. Their absorption features match the absorption peaks reported by Murray and co-workers as a minority fraction (the smallest size, $d = 1.2$ nm sub-population) of their high-temperature decomposition process.[3] This suggests that thermodynamic stability combined with pyridine etching can produce nearly monodisperse clusters of a critical size. This process is analogous to that discovered in the case of nanocrystals of Au etched by short-chain alkanethiols.[16]

Acknowledgment. This work was supported by the Division of Materials Science and Engineering, Office of Science, U.S. Department of Energy under Contract DE-AC04-AL8500. Sandia is a multiprogram laboratory operated by Sandia Corporation, a Lockheed-Martin Company, for the U.S. Department of Energy.

Supporting Information Available: Five spectra obtained during studies of the samples. This material is available free of charge via the Internet at http://pubs.acs.org.

References and Notes

(1) Henglein, A. *Chem. Rev.* **1989**, *89*, 1861−1873.

(2) (a)Lianos, P.; Thomas, J. K. *J. Colloid Interface Sci.* **1987**, *117*, 505. (b) Stiegerwald, M. L.; Alivisatos, A. P.; Gibson, J. M.; Harris, T. D.; Kortan, R.; Muller, A. J.; Thayer, A. M.; Duncan, T. M.; Douglass, D. C.; Brus, L. E. *J. Am. Chem. Soc.* **1988**, *110*, 3046−3050.

(3) Murray, C. B.; Norris, D. J.; Bawendi, M. G. *J. Am. Chem. Soc.* **1993**, *115*, 8706−8715.

(4) Norris, D. J.; Sacra, A.; Murray, C. B.; Bawendi, M. G. *Phys. Rev. Lett.* **1994**, *101*, 8455.

(5) Treadway, J. A.; Zehnder; D. A.; Schrier; M. D. U.S. Patent 6,815,064, Nov. 9, 2004.

(6) (a) Dabbousi, B. O.; Rodriguez-Viejo, J.; Mikulec, F. V.; Heine, J. R.; Mattoussi, H.; Ober, R.; Jensen, K. F.; Bawendi, M. G. *J. Phys. Chem. B* **1997**, *101*, 9463−9474. (b) Peng, X.; Schlamp, M. C.; Kadavanich, A. V.; Alivisatos, A. P. *J. Am. Chem. Soc.* **1997**, *119*, 7019−7029.

(7) Bawendi, M. G.; Jensen, K. F.; Dabbousi, B. O.; Rodriguez-Viejo, X.; Mikulec, F. V. U.S. Patent 6,322,901, Nov 27, 2001.

(8) Wilcoxon, J. P.; Provencio, P. *Proceedings of the SPIE conference on Optical Properties of Nanocrystals* **2002**, *4808*, 99−114.

(9) Ridley, B. A.; Nivi, B.; Jacobson, J. M. *Science* **1999**, *286*, 746.

(10) Wilcoxon, J. P.; Martin, J. E.; Provencio, P. *Langmuir* **2000**, *16*, 9912−9920.

(11) Wilcoxon, J. P.; Martin, J. E.; Provencio, P. *J. Chem. Phys.* **2001**, *115*, 998.

(12) Wilcoxon, J. P.; Craft, S. A. *Nanostruct. Mater*. **1997**, *9*, 85−88.

(13) (a) Nad, S.; Pal, H. *J. Phys. Chem. A* **2003**, *107*, 501−507. (b) Kubin, R. F.; Fletcher, A. N. *J. Lumin.* **1982**, *27*, 455−462.

(14) Yau, W. W.; Kirkland, J. J.; Bly, D. D. *Modern Size-Exclusion Liquid Chromatography*; Wiley-Interscience: New York, 1979.

(15) Platschek, V.; Schmidt, T.; Lerch, M.; Muller, G.; Spanhel, L.; Emmering, A.; Fricke, J.; Foitzik, A. H.; Langer, E. *Ber. Bunsen-Ges.Phys. Chem., Chem. Phys.* **1998**, *102*, 85−95.

(16) Wilcoxon, J. P.; Provencio, P. *J. Phys. Chem. B* **2003**, *107*, 12949−12957.